# Modelling Geometrical and Fluid-Dynamic Aspects of a Continuous Fluidized Bed Crystallizer for Separation of Enantiomers

Michael Mangold[1a], Dmytro Khlopov[b], Erik Temmel[b], Heike Lorenz[b], Andreas Seidel-Morgenstern[b]

[a] *Technische Hochschule Bingen, Berlinstraße 109, 55411 Bingen, Germany*
[b] *Max Planck Institute for Dynamics of Complex Technical Systems Sandtorstraße 1, 39106 Magdeburg, Germany*

**Abstract**

Continuous selective crystallization using mixed suspension mixed product removal (MSMPR) crystallizers is an attractive method for separating enantiomers. Recent experimental results confirm the feasibility of the approach, but also indicate that the operation conditions for nominal operation lie in a rather small window. A systematic analysis and an optimal design are needed to exploit the full potential of the method. In this contribution, a mathematical process model based on population balance equations is presented. In contrast to other studies in literature, the considered crystallizer is not a stirred tank, but has a conical shape that requires a spatially distributed model formulation. Parameter studies identify the key operation and design parameters for maximizing the mass of the product crystals and for shaping their size distribution. The proposed model focuses on geometrical and fluid-dynamic aspects, but at the current stage does not include purity aspects.

*Keywords:* enantiomers, separation, continuous crystallization, mathematical modelling, population balance equations, simulation

## 1. Introduction

Chiral substances or enantiomers consist of molecules which are not superimposable on their mirror image - like right hand and left hand. Chemical synthesis commonly produces a 50:50% mixture of the enantiomers of a chiral substance. Hence, the separation of such mixtures into the sterically pure components is of vital importance, since the two enantiomers may have completely different effects on living organisms (Stinson, 2001; Myerson, 2002). However, enantiomers exhibit identical physical properties due to the mirror symmetry, and simple separation

[1]Corresponding author. Tel. +49 6721 409 139 . E-mail m.mangold@th-bingen.de

techniques like distillation are not applicable, but more advanced methods are needed. Preferential crystallization has been found to be an attractive approach to this challenging problem, if the enantiomers form conglomerates (Alvarez and Myerson, 2010; Lorenz and Seidel-Morgenstern, 2014).

A robust crystallization process for the continuous production of particles with a defined size distribution in conically shaped crystallizers was proposed already in the 1970s by Midler (1975, 1976). Recently, the process has been combined with the technique of preferential crystallization and has been studied experimentally in detail (Binev et al., 2015; Binev, 2015; Binev et al., 2016). The in-situ production of seed material as suggested by Midler simplifies the operation in contrary to the continuous enantio-selective crystallization utilizing the MSMPR concept (Galan et al., 2015). Furthermore, permanent removal of possibly occurring nuclei of the counter-enantiomer increases process robustness and operating time. Hence, continuous production of pure enantiomers with an adjustable crystal size distribution is attainable.

Various process configurations and substances have been considered, and the feasibility of the process could be proven. However, it also turned out that the operation is quite delicate, and that the operation window is rather small. Therefore, optimizing the process based on experimental studies alone would be rather inefficient.

The most important goal of the process is to obtain crystals of high purity. This aspect has been modeled and investigated for different process configurations of coupled stirred tank crystallizers by Qamar et al. (2013); Vetter et al. (2015). It is not considered here. Instead, the contribution focuses on the additional degrees of freedom of a conical crystallizer compared to a stirred tank crystallizer. The spatial extension of the conical crystallizer causes a spatial dependency of the crystal distribution, which has to be accounted for in a mathematical model and does not exist in a stirred tank. By choosing a suitable crystallizer geometry, i.e. a crystallizer shape and a position for product removal, the spatial dependency may be exploited to design the size distribution of the product crystals. The aim of this contribution is to provide a process model that helps to obtain an understanding of the geometrical effects in combination with other operation parameters.

The following section introduces the details of the continuous crystallization process. Section 3 presents model assumptions and model equations. A simulation study based on the process model follows in Section 4. The contribution ends with some conclusions and an outlook in Section 5.

## 2. Process Description

The aims of the continuous enantioselective crystallization process are to grow crystals of one enantiomer while keeping the counter enantiomer in the liquid solution, to selectively extract crystals of a certain desired size, and to provide

the process continuously with fresh seed crystals. Therefore, a setup consisting of a feed tank, a crystallizer, and a device for seed generation, as sketched in Figure 1, is utilized. For further details on process conditions, the reader is referred to Binev et al. (2015); Binev (2015).

Selective crystallization is achieved by providing seed crystals of the desired enantiomer only. Hence, exclusively the desired dissolved stereoisomer is attached to the crystal surface due to the unique properties of the crystal lattice. Temperature and solute concentration in the crystallizer have to be chosen such that the crystallizer operates in the metastable zone. Then the supplied seed crystals are able to grow, but the nucleation of the counter-enantiomer is avoided to a certain extent.

The experimental set-up (Figure 1) is operated as follows: A solid racemic (50:50 mixture of both enantiomers) feed is provided in excess in a solution saturated at a certain temperature in the feed tank. The feed tank contains a clear racemic solution without crystals. The fresh solution is fed from the feed tank to the bottom of the crystallizer. By keeping the feed tank at a slightly higher temperature level than the crystallizer, the liquid in the column is super-saturated. An additional sieve between feed tank and crystallizer guarantees that the crystallizer feed is virtually free of particles. Subsequently, the process is seeded once *ex situ*. The feed flow rate is adjusted properly, so that a fluidized bed forms inside the crystallizer. Because the column has a conical shape, the fluid flow velocity is highest at the bottom of the crystallizer and decreases towards the top of the conical section. Therefore, the average size of the crystals in the fluidized bed decreases from bottom to top, as well. By choosing the position of the product outlet, a classifying product removal is attempted. Product crystals may either be withdrawn continuously or, as in the experiments by Binev et al. (2015), product samples are taken in a pulse-wise manner. The large crystals accumulating at the crystallizer bottom are withdrawn and sent to a mill or ultrasonic attenuator, where they are broken into smaller fragments and sent back to the crystallizer. In this way, the process generates the required seed crystals. Very small crystals move with the fluid flow and escape through the top of the crystallizer. This has a purifying effect, because it washes out undesired nuclei of the counter-enantiomer. The fines leaving the crystallizer are not lost, but dissolved on their way back to the feed tank. The valuable material is in this way recycled for the crystallization process.

## 3. Model Equations

Mathematical models of the considered process were published by Palis et al. (2013); Mangold et al. (2015); Binev et al. (2016). The process model presented in the following is based on those previous publications. The model consists of a population balance for the particles in the crystallizer, a mass balance for

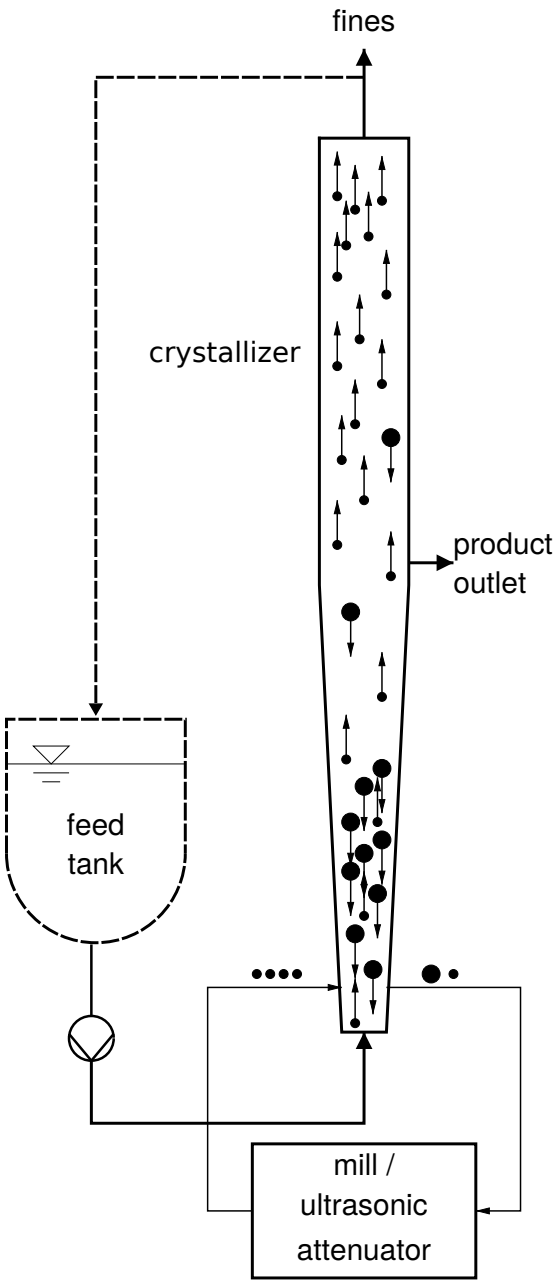


Figure 1: Sketch of a continuous process for enantioselective crystallization consisting of a feed tank, a crystallizer, and a mill for continuous seed generation.The feed tank and the recycle loop (drawn as dashed lines) are not part of the process model.

the solute in the liquid phase, and a population balance for the particles in the disperser / mill.

Figure 2 gives a schematic representation of the process showing the flow rates and the main geometrical parameters.

The main model assumptions are:

- The crystallizer consists of a cylindrical upper part, and a conical lower part.
- The product outlet is located at a position $x = x_P$; the product is removed from the crystallizer with a constant flow rate $\dot{V}_{prod}$;
- Spatial gradients perpendicular to the crystallizer axis $x$ in the direction of the fluid flow are negligible;
- The composition of the feed tank does not change over time. This might be achieved by permanently adding fresh solute to the feed tank in a controlled manner in order to compensate the depletion of solute due to product removal. It has the consequence that the recycle from the crystallizer to the feed tank has no effect on the simulation results. The reason for this assumption is to obtain non-trivial steady state solutions in the model, whereas a varying feed tank composition would send the model system on a permanent transient and eventually to a trivial steady state without a solid phase.
- the liquid enters the crystallizer at the bottom $x = 0$ with a volumetric flow rate $\dot{V}_{in}$; the incoming liquid does not contain any crystals;
- plug flow is assumed, i.e. constant liquid flow velocity over the cross-section of the crystallizer;
- the conditions in the crystallizer are approximately isothermal;
- crystals grow in the crystallizer, but no nucleation, agglomeration or breakage occurs;
- The size of the crystals is described by a characteristic length $L$, which indicates the diameter of spheres with the same volume as the crystals. The behaviour of the crystals in the flow field depends on their actual shape and is captured by a sphericity parameter $\Psi$.

*Population balance for the particles in the crystallizer.* The solid phase in the crystallizer is described by a number size density $n(x, L, t)$. A population balance

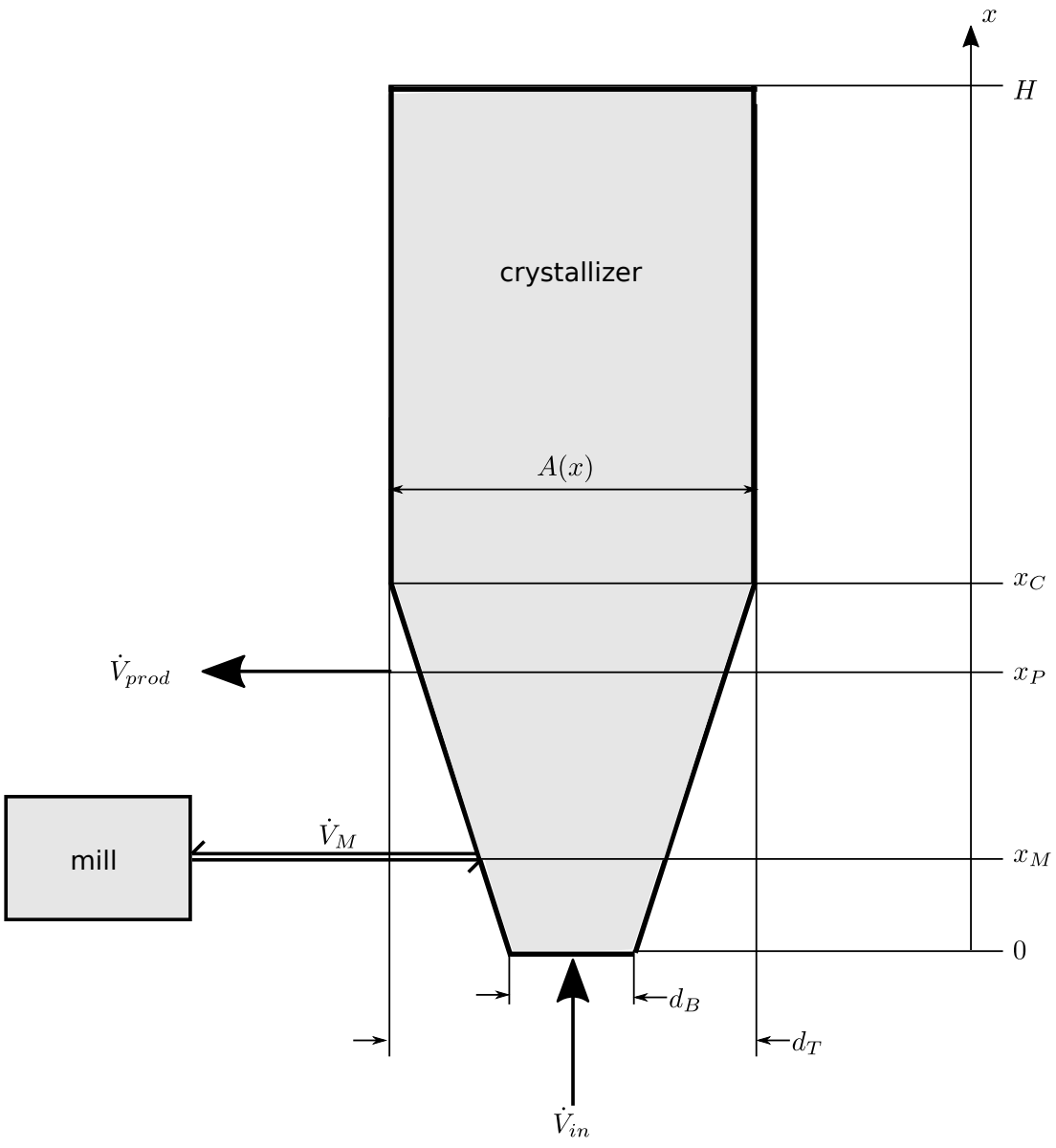


Figure 2: Schematic representation of the selective crystallization process

gives

$$
\begin{aligned}
A(x)\left.\frac{\partial n}{\partial t}\right|_{x,L,t} &= -\frac{\partial}{\partial x}\left(A(x)\, v_P(x,L,t)\, n(x,L,t)\right) \\
&\quad + D\frac{\partial}{\partial x}\left(A(x)\left.\frac{\partial n}{\partial x}\right|_{x,L,t}\right) \\
&\quad - A(x)\, G(c)\left.\frac{\partial n}{\partial L}\right|_{x,L,t} \\
&\quad + \dot{V}_M\left(n_M(L,t) - n(x,L,t)\right)\delta(x - x_M)
\end{aligned}
\tag{1}
$$

$$(0 < x < H, \quad 0 < L, \quad t > 0)$$

with boundary conditions

$$
\begin{aligned}
v_P(0,L,t)\, n(0,L,t) - D\left.\frac{\partial n}{\partial x}\right|_{0,L,t} &= 0 && (2)\\
\left.\frac{\partial n}{\partial x}\right|_{H,L,t} &= 0 && (3)\\
n(x,0,t) &= 0 && (4)
\end{aligned}
$$

and initial conditions

$$n(x,L,0) = n_0(x,L). \tag{5}$$

The first term on the right-hand side of (1) describes the convective transport of particles with a velocity $v_P(x,L,t)$, which is size dependent and in general different from the liquid flow velocity. $A(x)$ is the cross-sectional area of the crystallizer. The second term stands for particle transport by dispersion. The third term is due to crystal growth described here by a first order growth rate $G(c)$ given as

$$G(c) = G_0\frac{c - c_{sat}}{c_{sat}} = G_0\,\sigma, \tag{6}$$

where $c$ is the mass fraction of the solute in the liquid phase, and $c_{sat}$ is the solute mass fraction in the saturated liquid. The fourth term describes the mass exchange with the mill; $x_M$ denotes the position of the exchange along the crystallizer axis; $\dot{V}_M$ is the volume flow to and from the mill; $n_M(L,t)$ is the number size density of the particles in the mill.

*Mass balance for the solute in the liquid phase.* The mass balance for the solute in the liquid phase of the crystallizer reads

$$\begin{aligned} A(x)\frac{\partial}{\partial t}\left(\epsilon(x,t)\ c(x,t)\right) &= -\frac{\partial}{\partial x}\left(\dot{V}(x)\ c(x,t)\right) \\ &\quad +\frac{\partial}{\partial x}\left(A(x)\ \epsilon(x,t)\ D\ \frac{\partial c(x,t)}{\partial x}\right) \\ &\quad +\frac{\rho_P}{\rho_f}\int_0^\infty A(x)\ G(c)\ \left.\frac{\partial n}{\partial L}\right|_{x,L,t}\frac{\pi}{6}L^3\ dL. \end{aligned} \tag{7}$$

The volume fraction of the fluid $\epsilon(x,t)$ on the left-hand side of (7) is given by

$$\epsilon(x,t) = 1 - \int_0^\infty n(x,L,t)\frac{\pi}{6}L^3\ dL. \tag{8}$$

The three terms on the right-hand side of (7) stand for convective transport with

$$\dot{V}(x) = \begin{cases} \dot{V}_{in} & \text{for } x < x_P \\ \dot{V}_{in} - \dot{V}_{prod} & \text{for } x > x_P \end{cases}, \tag{9}$$

dispersion, and mass transfer to the solid phase, respectively.

*Velocity of the particles in the crystallizer.* The particle velocity $v_P(x,L,t)$ is described by the classical model by Richardson and Zaki (1954), as this model is rather simple, but nevertheless has been shown by Binev et al. (2015) to describe the experimentally observed particle behaviour with reasonable accuracy.

To obtain $v_P$, first the Archimedes number (describing the ratio between buoyancy and friction force on a particle of size $L$) is calculated from

$$Ar(L) = \frac{g\ \hat{L}^3\ \rho_f\ (\rho_P - \rho_f)}{\mu_f^2}, \tag{10}$$

where $\hat{L} = L/\Psi$ is the size of an equivalent spherical particle, $\Psi$ being a shape dependent sphericity parameter. The fluid velocity $v_{eq}$ needed to keep a single particle of size $L$ in equilibrium follows from

$$v_{eq}(L) = \frac{Re_{eq}(L)\mu_f}{\hat{L}\rho_f}, \tag{11}$$

with the Reynolds number (Gibilaro, 2001)

$$Re_{eq}(L) = \left(-3.809 + \left(3.809^2 + 1.832\, Ar(L)^{0.5}\right)^{0.5}\right)^2. \tag{12}$$

For higher particle densities, $v_{eq}$ has to be corrected in the following way to account for particle-particle interactions:

$$v_{eq}^*(x, L, t) = v_{eq}(L)\ \epsilon(x, t)^{m(L)} \tag{13}$$

with

$$\frac{4.8 - m(L)}{m(L) - 2.4} = 0.043\ Ar(L)^{0.57}. \tag{14}$$

Finally, the particle velocity $v_P(x, L, t)$ is computed from

$$v_P(x, L, t) = \frac{\dot{V}}{A(x)} - v_{eq}^*(x, L, t). \tag{15}$$

*Population balance for particles in the mill.* In the laboratory experiments, a high speed dispersing instrument[2] is used to break the crystals at the bottom of the crystallizer into small fragments, which is different from former studies. As a simple model of the disperser, we use a standard population balance model with breakage, similar to the model of a screen mill by Reynolds (2010). The purpose of this model is to reproduce the experimentally observed input-output behaviour of the disperser with an accuracy sufficient to capture the influence of the mill on the crystallization process. The model is purely phenomenological and not meant to provide insight in the physical processes inside the disperser. More detailed models with a larger validity range have been proposed e.g. by Luciani et al. (2015), but are outside the scope of this work.

Assuming perfect mixing in the disperser, the population balance equation for the number size density $n_M(L, t)$ in the disperser reads

$$\left.\frac{\partial n_M}{\partial t}\right|_{L,t} = \int_L^\infty b(L, l)\ S(l)\ n_M(l, t)\ dl - S(L)\ n_M(L, t) + \frac{\dot{V}_M}{V_M}\left(n(L, t) - n_M(L, t)\right) \tag{16}$$

The Hill Ng breakage distribution function (Hill and Ng, 1996; Diemer et al., 2005) is used for $b(L, l)$:

$$b(L, l) = K\ \frac{1}{l}\left(\frac{L}{l}\right)^{3\,(q-1)}\ \left(1 - \left(\frac{L}{l}\right)^3\right)^{r-1}, \quad r = q\,(p-1). \tag{17}$$

The parameter $p$ may be interpreted as the number of daughter fragments after a breakage event, $q$ is a sharpness parameter (Diemer et al., 2005), and $K$ is a scaling constant chosen such that mass is conserved.

For the breakage kernel $S(L)$, the expression

$$S(L) = S_0\ H(L - L_c) \tag{18}$$

[2]IKA T25 digital ULTRA-TURRAX with a S 25 KV - 18 G dispersing element.

with Heaviside function $H(L - L_c)$ is used. The critical particle size $L_c$, above which breakage may occur, is chosen as the gap between rotating blade and stationary parts of the disperser.

The model of the mill contains three kinetic parameters $p$, $q$, and $S_0$ to be identified from experiments. The parameter estimation procedure applied is sketched in Appendix A.

*Numerical solution.* Using the method of lines, the model equations are discretized on a grid with 110 equidistant grid points on the $x$ coordinate and 80 equidistant grid points on the $L$ coordinate. The resulting ODE system is implemented in Octave. The steady state solutions are obtained by a time integration with the LSODE integrator using the explicit Adams Bashforth method. The integration is stopped when the relative mass defect, i.e. the ratio between the sum of all mass flows across the system boundary and the mass flow into the system, falls below a threshold of $10^{-3}$.

## 4. Simulation results

This section discusses the steady state solution of the crystallization process and its dependence on the main operation and design parameters. After discussing a reference solution resulting from a nominal parameter set, we investigate the influence of important operation parameters that may be changed for a given apparatus design and given substances. These are the three volume flow rates $\dot{V}_{in}$, $\dot{V}_{Prod}$, and $\dot{V}_M$. After that, parameter changes are considered that would require a constructive modification of the process. Parameters related to the crystallizer geometry and to the properties of the mill belong to this category. Finally, the effect of changing solute and solvent is studied by varying the growth rate constant $G_0$.

### *4.1. Nominal case*

The model parameter values in the nominal case are in agreement with the experiments by Binev (2015); Binev et al. (2016). They are listed in Table 1. It is assumed that the product is removed continuously from the crystallizer with a constant flow rate $\dot{V}_{prod}$. This is in contrast to the experimental conditions, where the product is extracted in a pulse-wise manner. Figure 3 shows the simulated profile of the number size distribution $n(x, L)$ under nominal steady state conditions. The green line indicates the position of the product outlet, which is at the end of the conical part of the crystallizer. The yellow line shows the size of particles whose velocity $v_P$ is equal to zero, i.e. they are in equilibrium with the fluid flow. Because of the conical shape of the crystallizer, the yellow equilibrium line moves to larger particle sizes towards the crystallizer bottom, where the diameter is most narrow and the fluid flow velocity is highest. The particles in equilibrium have a constant size in the upper cylindrical part of the crystallizer.

| | |
|---|---|
| $D$ | $10^{-5}\ \mathrm{m^2\,s^{-1}}$ |
| $d_B$ | 15 mm |
| $d_T$ | 30 mm |
| $G_0$ | $3.37 \cdot 10^{-7}\ \mathrm{m\,s^{-1}}$ |
| $H$ | 110 cm |
| $L_C$ | 300 $\mu$m |
| $p$ | 10.8 |
| $q$ | 0.2 |
| $S_0$ | 0.072 |
| $V_M$ | 20 ml |
| $\dot{V}_{in}$ | 9 l/h |
| $\dot{V}_M$ | 21 l/h |
| $\dot{V}_{prod}$ | 2.7 l/h |
| $x_c$ | 51.5 cm |
| $x_M$ | 0.5 cm |
| $x_P$ | 54.5 cm |
| $\mu_f$ | $6.5 \cdot 10^{-4}\ \mathrm{kg\,m^{-1}\,s^{-1}}$ |
| $\rho_F$ | $994.6\ \mathrm{kg\,m^{-3}}$ |
| $\rho_P$ | $1410\ \mathrm{kg\,m^{-3}}$ |
| $\Psi$ | 0.5 |

Table 1: Model parameter values in the nominal case

The equilibrium size is much smaller above the product outlet than below due to the reduced fluid flow velocity. The product outflow has a strong effect on the particle equilibrium size, which changes rapidly in the segment immediately below the outlet point.
Most particles group around the equilibrium line in the lower part of the crystallizer. There are hardly particles above the product outlet, because the reduced fluid flow makes larger particles sink back into the lower part. As a consequence, the particle density is highest shortly below the product outlet, as can be seen in Figure 4.
Figure 5 shows the particle size distribution in the product (position $x_P$) as an important quantity for the application of the crystallization process. The sizes of most product particles lie between two peaks of the number density function in Figure 5: one peak at around 200 $\mu$m corresponding to the equilibrium particle size below the product outlet, and a second peak around 50 $\mu$m corresponding to the equilibrium size above the product outlet. In addition, the product flow contains a share of very small particles generated by the breakage events in the mill. As the method to extract the product and the seed generation in the simulation differ from the experiments by Binev (2015), a direct comparison with experimental data is difficult. Nevertheless, the size distribution of the product crystals reported in (Binev, 2015) is at least in the same order of magnitude as in the simulations.
The size distribution of particles escaping through the top of the crystallizer ($x = H$) is depicted in Figure 6. This distribution has two maxima: one around the equilibrium size of 50 $\mu$m, and the other at very small particle sizes. To some extent, the wash-out of crystals at the top reduces the efficiency of the process, as these crystals have to be dissolved and recycled back into the crystallizer. On the other hand, the escape of small crystals of the counter-enantiomer, which may nucleate in reality, but are not considered in the simulation, has a purifying effect on the process and increases its long-term stability.

### *4.2. Influence of the fluid flow rate*

The dependence of the steady state solution on the flow rate of the liquid $\dot{V}_{in}$ is studied in the following. When varying $\dot{V}_{in}$, the ratio between the product flow rate $\dot{V}_{prod}$ and $\dot{V}_{in}$ is kept constant, i.e. the ratio between the residence time of the fluid in the lower part of the crystallizer (below the product outlet) and the residence time in the upper part does not change.

Figure 7 shows that the size of the product crystals grows with an increasing flow rate, because at higher fluid flow velocities, the particles must have a larger size in order not to be washed out of the crystallizer. However, this effect is not very strong. As a consequence, the total product mass flow changes nearly linearly over a wide range of $\dot{V}_{in}$, as is shown in Figure 8. Only if the flow rate exceeds a threshold of about 29 l/h, the flow velocity becomes so large that most

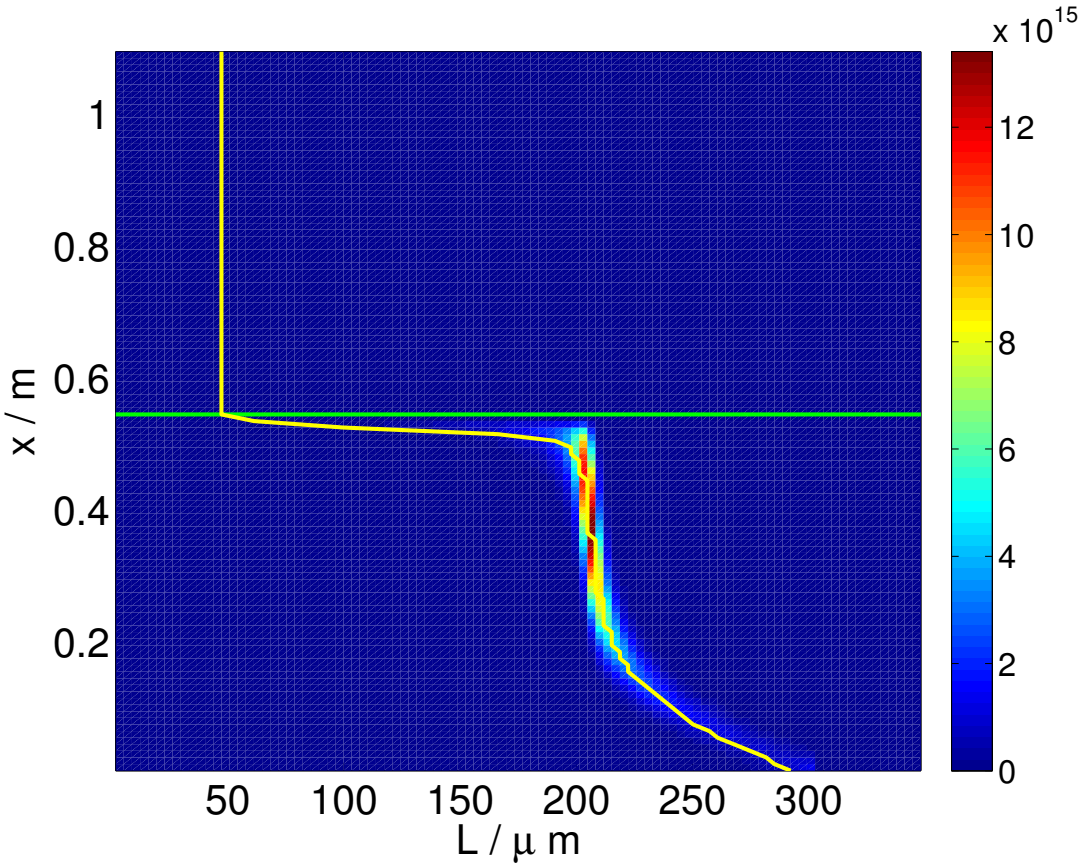


Figure 3: Steady state number size density $n(x, L)$ under nominal conditions; green line = position of product outlet $x_P$; yellow line = size of particles in equilibrium with the fluid flow.

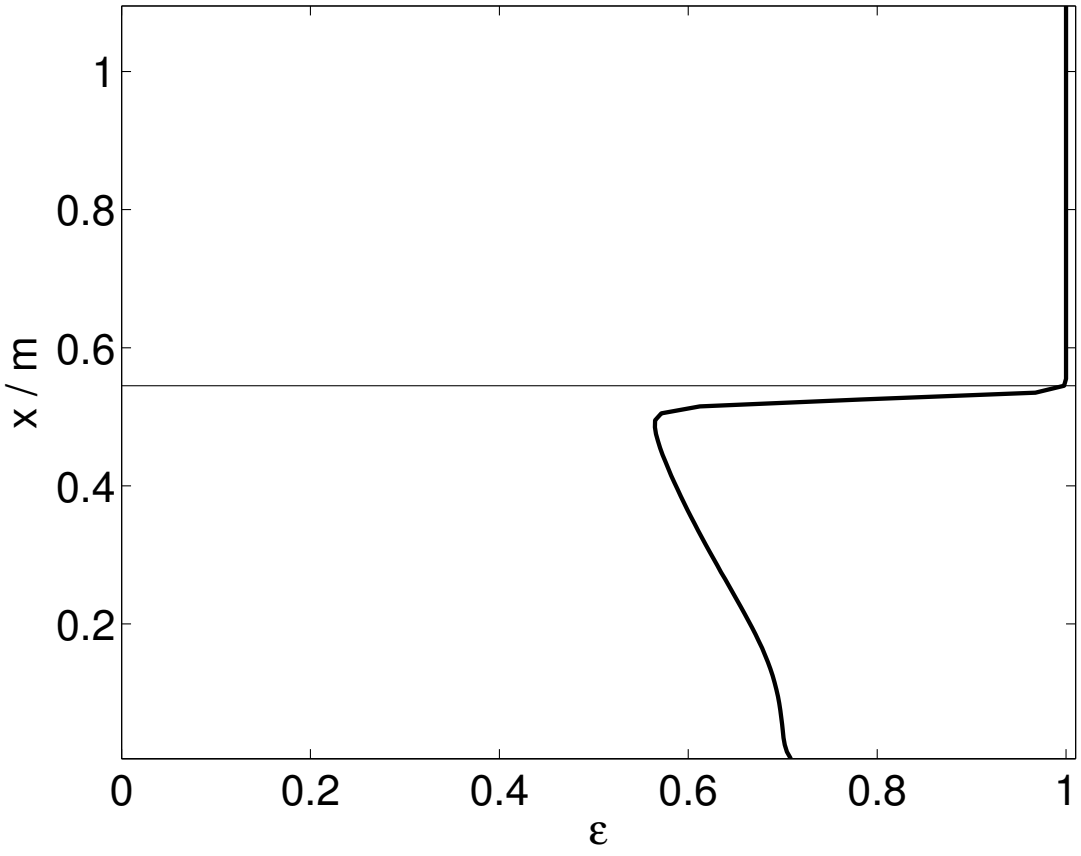


Figure 4: Fluid volume fraction $\epsilon(x)$ under nominal steady state conditions; the thin horizontal line marks the position of the product outlet $x_P$.

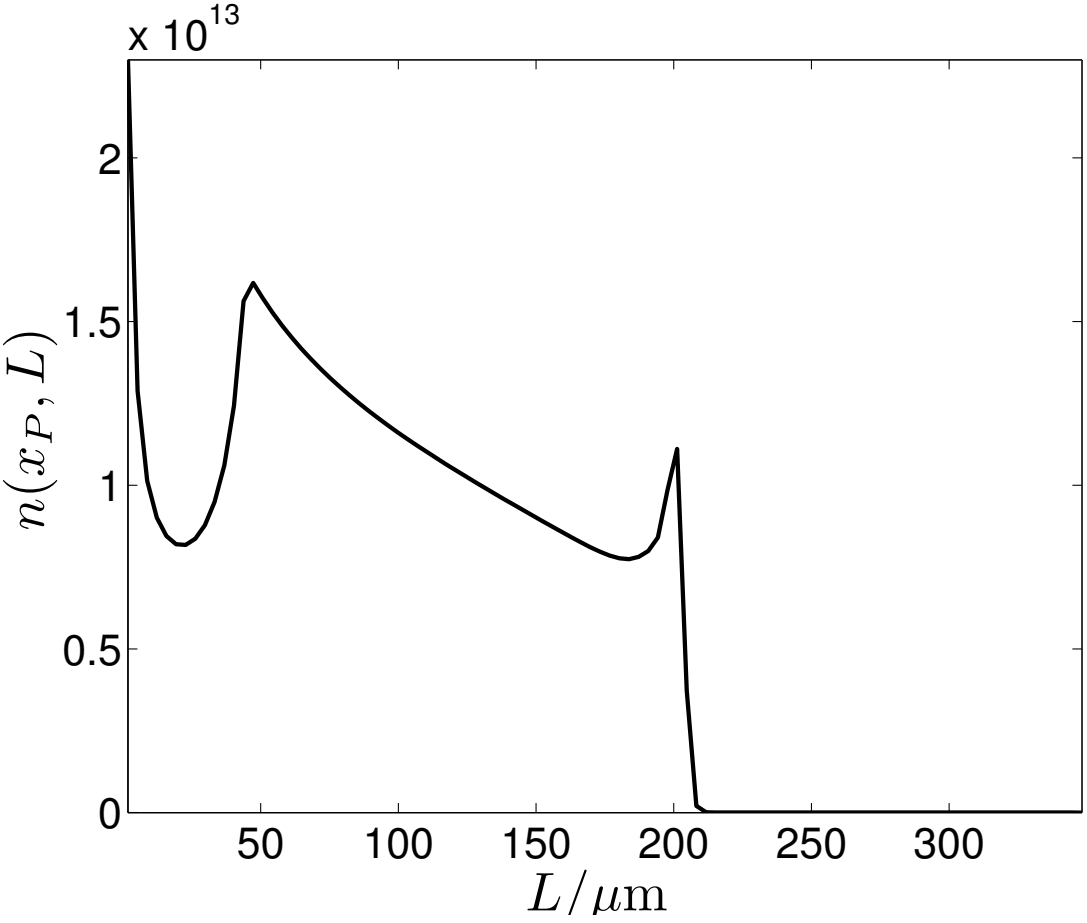


Figure 5: Number size density in the product flow $n(x_P, L)$ under nominal steady state conditions.

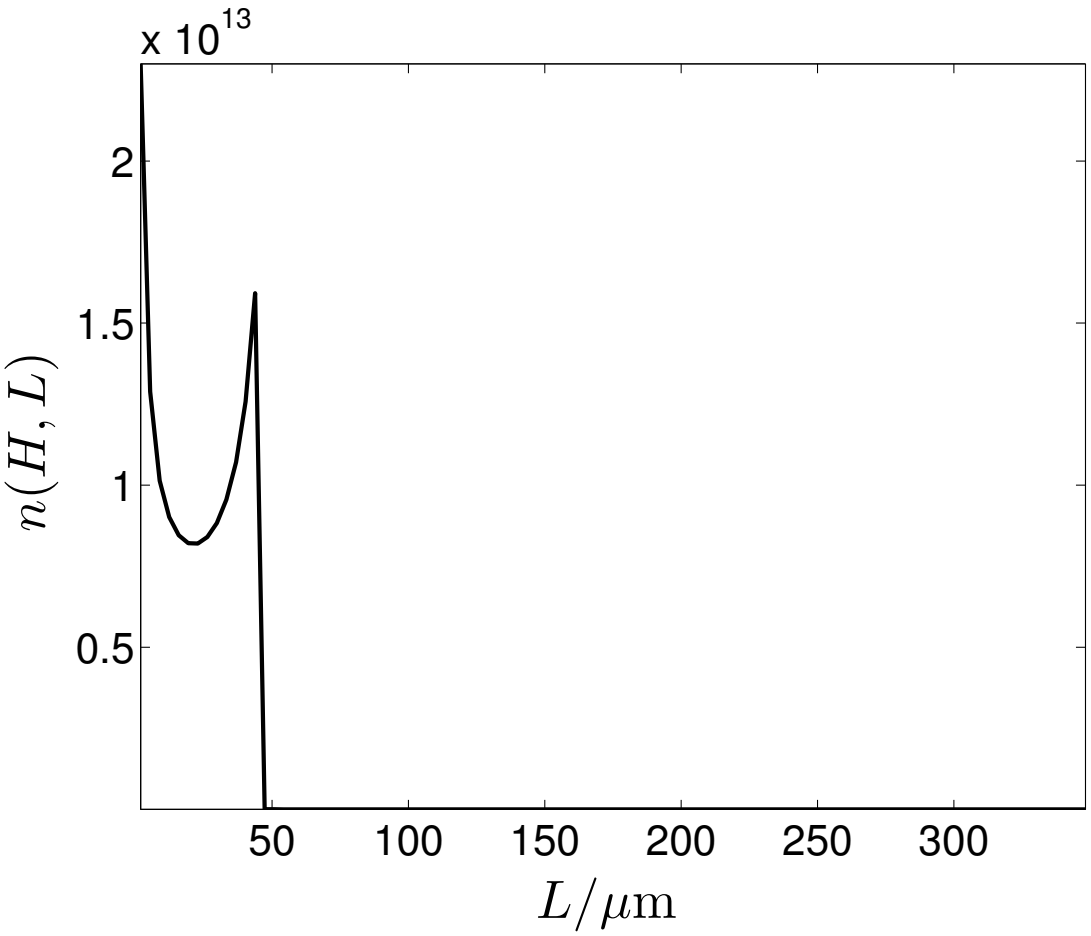


Figure 6: Number size density at the top of the crystallizer $n(H, L)$ under nominal steady state conditions.

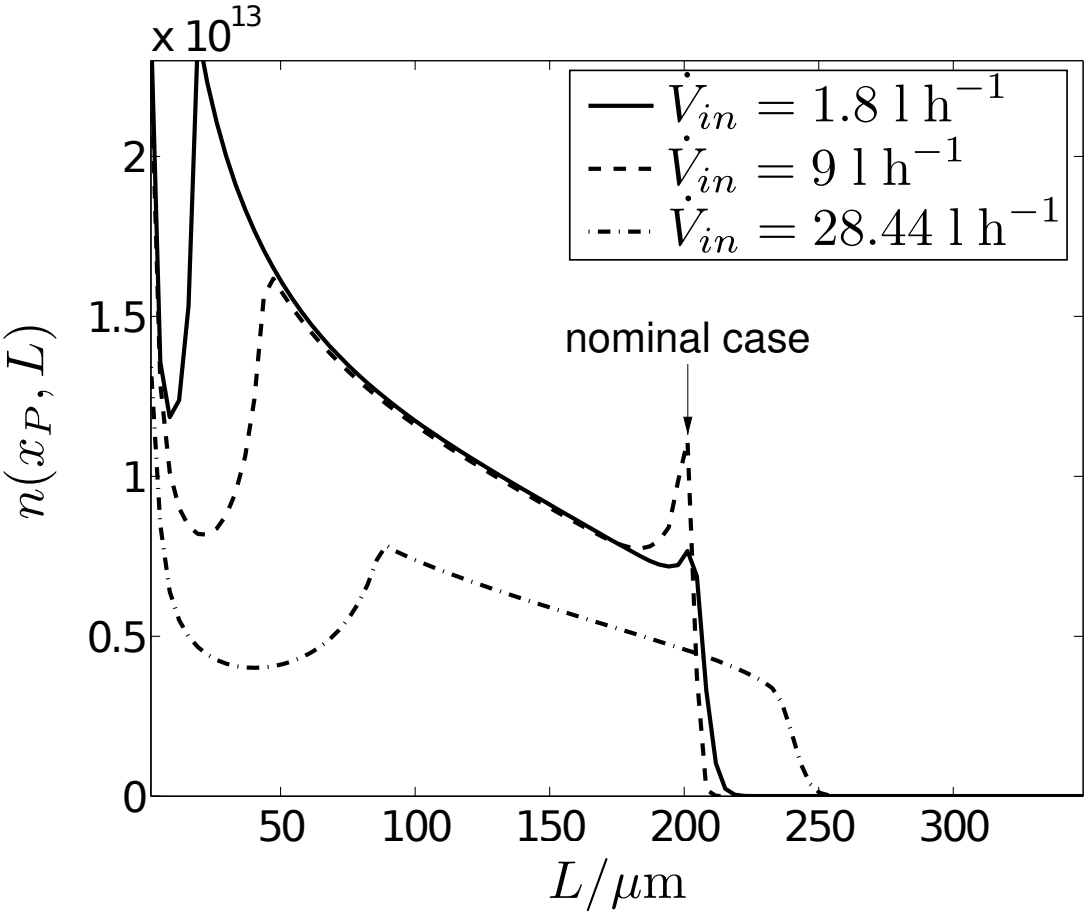


Figure 7: Number size densities of the crystals in the product flow $n(x_P, L)$ for three different fluid flow rates $\dot{V}_{in}$ at a constant ratio $\dot{V}_{Prod}/\dot{V}_{in} = 0.3$. The fluid flow rates $\dot{V}_{in}$ correspond to residence times of 425 s, 85 s, 27 s, respectively, in the conical part of the crystallizer, and to 1182 s, 237 s, 75 s, respectively, in the cylindrical part.

of the crystals are taken out of the crystallizer with the fluid flow, and the yield drops quickly.

*4.3. Influence of the product flow rate*

In the following, the product flow rate is varied, while the inlet flow rate at the bottom of the crystallizer is kept constant, i.e. the residence time of the fluid changes only in the cylindrical part. The first observation is that the crystal size distribution in the product flow hardly changes for a wide range of product flow rates, however, the absolute value of the number size density increases with a decreasing product flow rate (see Figure 9). As a consequence, the total mass flow of crystals in the product stream is nearly constant for a product flow rate between 2.7 l/h and about 0.02 l/h, as is shown in Figure 10.

As was discussed above, the product outlet forms a kind of barrier for the

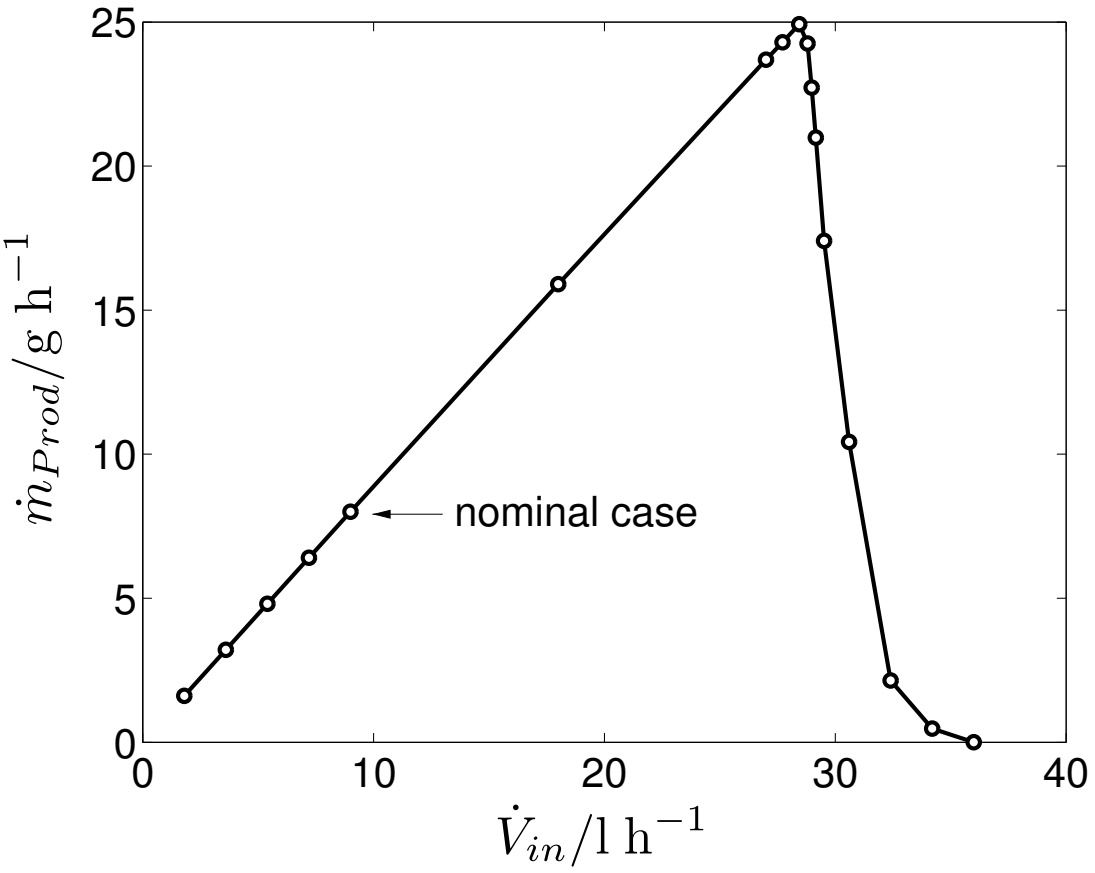


Figure 8: Product mass flow $\dot{m}_{prod}$ as a function of the flow rate $\dot{V}_{in}$ at a constant ratio $\dot{V}_{Prod}/\dot{V}_{in} = 0.3$; flow rates $\dot{V}_{in}$ correspond to residence times between 21 s and 425 s in the conical crystallizer part..

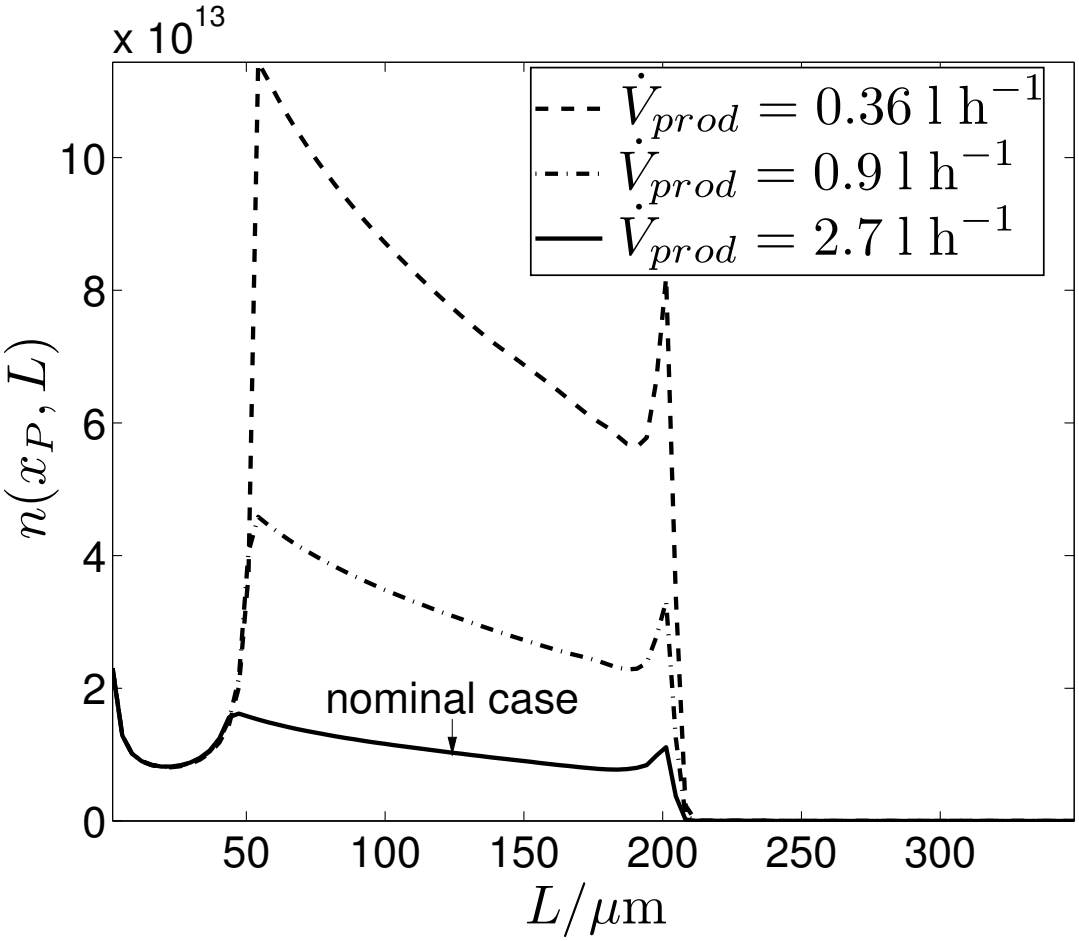


Figure 9: Number size densities of the crystals in the product flow $n(x_P, L)$ for three different product flow rates $\dot{V}_{Prod}$ ($\dot{V}_{in} = 9\,\mathrm{l/h}$), corresponding to a residence time of 85 s in the conical part, and 237 s, 184 s, 172 s, respectively, in the cylindrical part.

crystals below the outlet. The larger crystals are not able to pass this barrier, because the fluid flow velocity and the drag caused by the fluid are smaller above the outlet, and larger crystals sink back into the lower part. However, for very small product flow rates, this effect becomes marginal: The crystals tend to arrange themselves in the upper cylindrical part of the crystallizer, where the diameter is larger, and, in this case, the drag is smaller. As an example, Figure 11 shows the number size density in the crystallizer for a very small product flow rate. The product flow rate of about 0.02 l/h, below which the product mass flow drops quickly, marks the boundary between the flow regime, where most crystals are located below the product outlet (Figure 3), and the flow regime, where the majority of crystals is above the product outlet Figure (11). Figure 12 shows that very small product flow rates may be attractive, if a narrow size distribution of the product is more important than a high productivity.

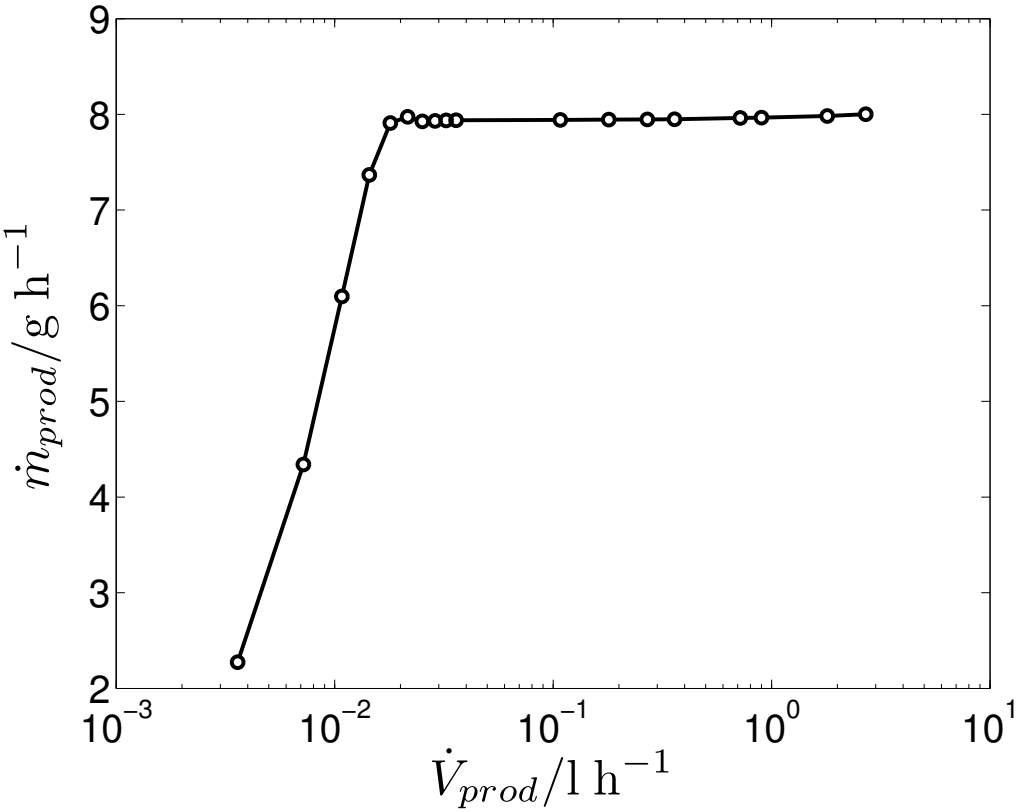


Figure 10: Product mass flow $\dot{m}_{Prod}$ as a function of the product flow rate $\dot{V}_{Prod}$.

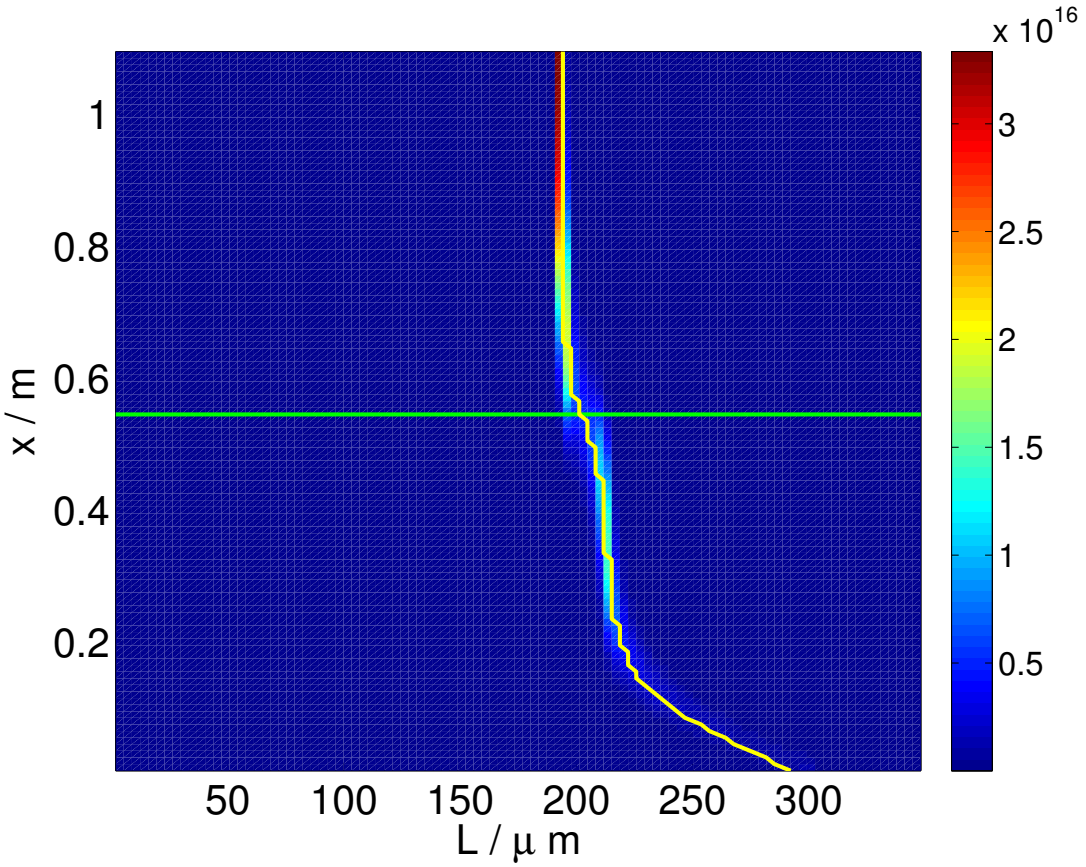


Figure 11: Steady state number size density $n(x, L)$ for $\dot{V}_{Prod} = 0.0036\ 1\mathrm{h}^{-1}$; green line = position of product outlet; yellow line = size of particles in equilibrium with the fluid flow.

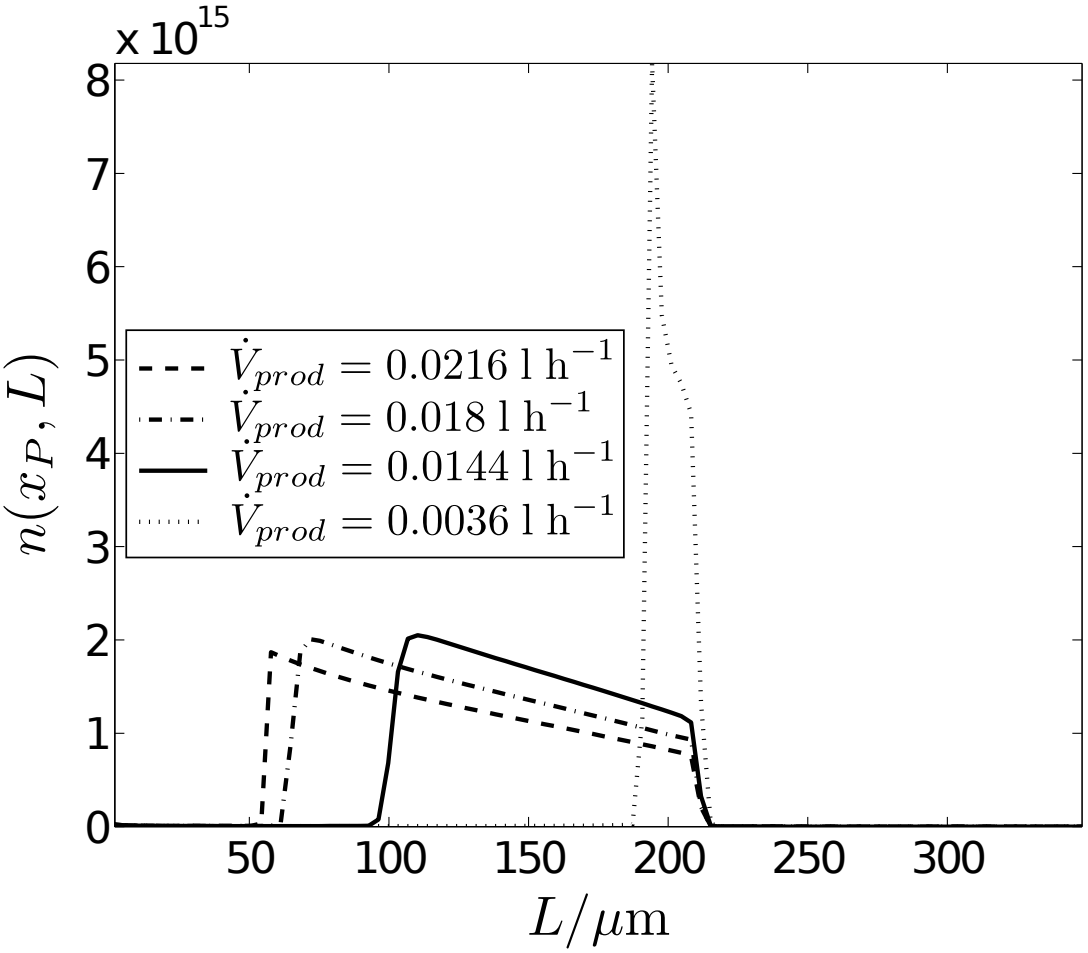


Figure 12: Number size densities of the crystals in the product flow for small product flow rates $\dot{V}_{Prod}$ ($\dot{V}_{in} = 9$ l/h): a narrow size distribution is achieved, albeit at the expense of productivity.

*4.4. Influence of the flow rate to the mill*

The third flow rate that has to be chosen is the flow rate to and from the mill. The mill is required, because it crushes large crystals at the crystallizer bottom and introduces new seeding crystals into the process. Without the mill, large crystals would accumulate in the lowest part of the crystallizer, and the upper parts would contain no crystals, at all. However, it turns out, that above a certain threshold, a change of the flow rate to and from the mill has no notable effect on the steady state behaviour of the process. In the simulations, it is possible to reduce this flow rate from the nominal value of 21 l/h down to 0.4 l/h without a visible change of the steady state solution.

*4.5. Influence of the properties of the mill*

The seed generation can be modified by changing the constructive parameters of the disperser like the gap between rotor and stator. To capture these effects in a simple manner, the parameter $L_C$ for the critical breakage size is varied. The simulation results in Figure 13 show that the size distribution of the seed, which is directly related to $L_C$ , is a strong lever for controlling the size of the product crystals. A smaller breakage size $L_C$ causes smaller product crystals. The total number of product crystals increases, and, therefore, the total product mass flow remains approximately constant in the considered parameter range. This means that by choosing $L_C$ one may adjust the product size distribution without strongly affecting the productivity of the process.

*4.6. Influence of the crystallizer geometry*

The crystallizer consists of two parts: a conical part meant to sort the crystals according to their crystal size and to enable a classifying product removal, and a cylindrical upper part, whose function is mainly to collect crystals not removed by the product outlet. In the following simulations, the geometry is modified in two ways: First, the diameter $d_T$ at the top of the conical part is increased by a factor of $\sqrt{2}$ in order to amplify the effect of the changing diameter in the cone. Second, the cylindrical part is shortened, as the simulation results revealed that the cylinder plays a minor role for the process behaviour.

In an attempt to exclude the influence of varying residence times due to changing the geometrical parameters, the flow rates $\dot{V}_{in}$ and $\dot{V}_{Prod}$ are adjusted such that the average fluid flow velocity in the empty ($\epsilon = 1$) conical part and in the empty cylindrical part are the same for the new geometry as for the nominal geometry, i.e.

$$\left.\frac{\dot{V}_{in}}{\frac{1}{x_C}\int_0^{x_C}\frac{\pi}{4}\,d(x)^2\,dx}\right|_{\text{new geometry}} = \left.\frac{\dot{V}_{in}}{\frac{1}{x_C}\int_0^{x_C}\frac{\pi}{4}\,d(x)^2\,dx}\right|_{\text{nominal geometry}}, \quad (19)$$

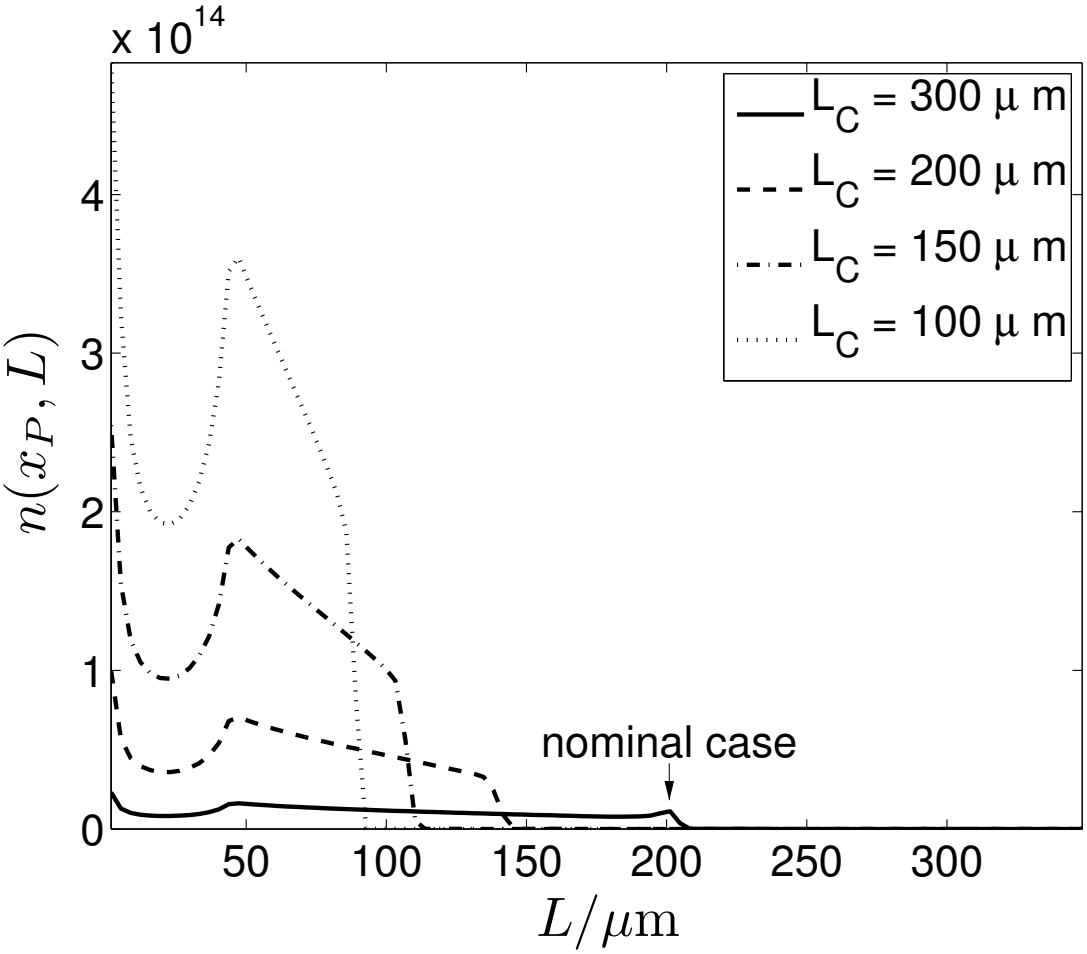


Figure 13: Dependency of the product size distribution $n(x_P, L)$ on the critical breakage size $L_C$ in the mill.

| | |
|---|---|
| $d_T$ | 42 mm |
| $H$ | 81 cm |
| $\dot{V}_{in}$ | 15.2 l/h |
| $\dot{V}_{prod}$ | 2.6 l/h |

Table 2: Parameter values for the modified geometry; parameters not listed are identical to the nominal case.

and

$$\left.\frac{\dot{V}_{in} - \dot{V}_{Prod}}{\frac{\pi}{4}\, d_T^2}\right|_{\text{new geometry}} = \left.\frac{\dot{V}_{in} - \dot{V}_{Prod}}{\frac{\pi}{4}\, d_T^2}\right|_{\text{nominal geometry}} . \qquad (20)$$

The modified parameters are listed in Table 2. A further geometrical design parameter is the position of the product outlet $x_P$. The simulation results contained in Figure 14 allow assessing the effect of the crystallizer geometry on the product size distribution. A classifying effect of the outlet position is mainly observed, when the product outlet position is very low ($x_P < 14.5$ cm). This is in agreement with the number size densities in Figure 3 and 11, which indicate that the particle size varies most strongly in the lowest part of the crystallizer. The classifying effect of the outlet position is stronger for the new geometry, because the crystallizer diameter and hence the fluid flow velocity change more strongly with the crystallizer position $x$.

### *4.7. Influence of the crystal growth rate*

In a last set of simulations, the sensitivity of the process towards the properties of solute and solvent is studied. In the rather simple process model, the solubility only enters the crystal growth rate (6) with a single parameter $G_0$, which has been varied in the simulations. The result is that the process behaviour depends only weakly on the growth rate (see Figure 15). Even if $G_0$ is varied over two orders of magnitude, the number size density of the product crystals changes only slightly. The same holds for the product mass flow. One may conclude that the process is dominated by fluid dynamics and mechanical effects and depends only to a smaller extent on the physico-chemical properties of the substances. The experiments by Binev et al. (2015); Binev (2015); Binev et al. (2016) proved operability of the process for a number of substances and confirm the general trend of these theoretical results.

## 5. Conclusions

The considered process of preferential crystallization in fluidized bed crystallizer is a feasible approach for the continuous selective crystallization of enantiomers. It is attractive for many separation problems. The process possesses

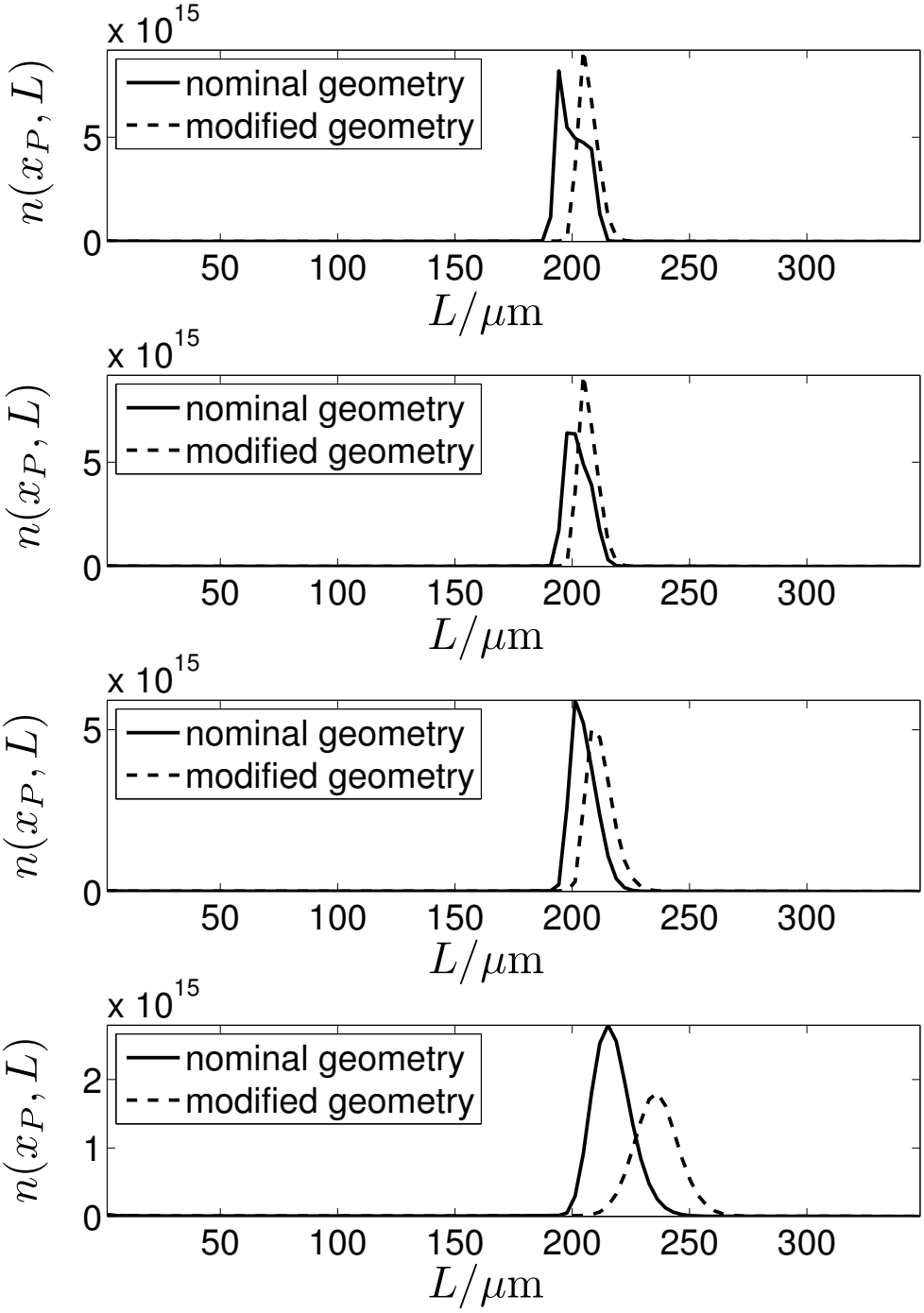


Figure 14: Effect of the crystallizer geometry on the product size distribution. The four diagrams show results for (from top to bottom) $x_P = 54.5$ cm, $x_P = 34.5$ cm, $x_P = 24.5$ cm, $x_P = 14.5$ cm. The product flow rate is chosen as $\dot{V}_{Prod} = 0.0036\,\mathrm{l\,h^{-1}}$.

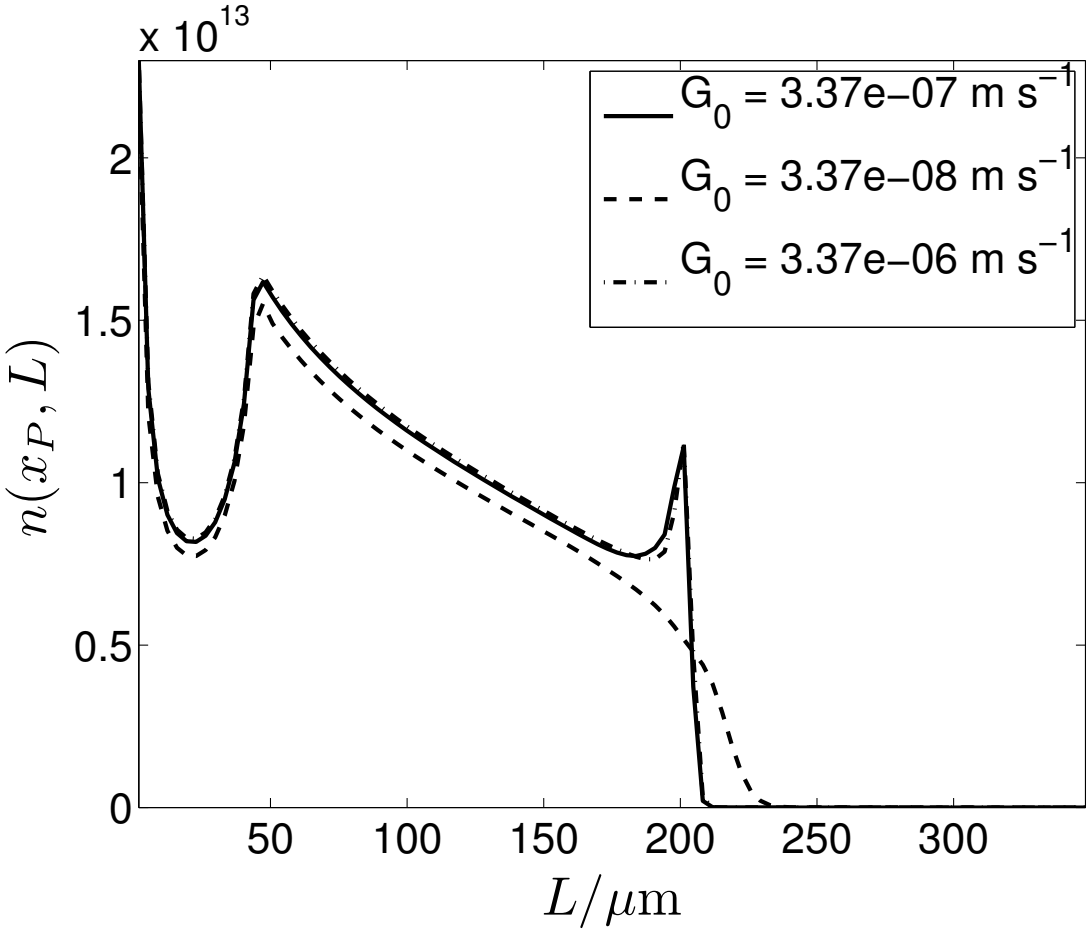


Figure 15: Dependency of the product size distribution on the crystal growth rate constant $G_0$.

various operation and design parameters that can be adjusted to tune the performance of the process. Two performance criteria have been considered in this work: the productivity, defined as the mass of crystals produced in a certain time, and the size distribution of the produced crystals as a measure for the product quality.

It is found that in particular the inlet flow rate has a strong influence on the productivity - there is an optimum value, where the mass flow of product crystals reaches a maximum. The inlet flow rate also has some effect on the product size distribution, but this effect is smaller.

The product flow rate hardly has an effect on the productivity and the product size distribution, as long as it is above a certain threshold. This may be useful, if the continuous crystallizer is part of a larger production process, because the product flow rate can be adjusted to the needs of the downstream devices. If the product flow rate is below the mentioned threshold, its variation allows to sharpen the product size distribution.

More effective means to change the product size distribution are modifications of the crystallizer geometry (diameters and position of the product outlet), and modifications of the mill affecting the size distribution of the seeds. On the other hand, the flow rate through the mill is found to have only a minor effect on the process. One only has to make sure that it exceeds a certain minimum.

Future work will concern the refinement of the model in two respects. First, the simulations indicate that the flow field close to the product outlet may have a strong influence on the product size distribution and may require a more detailed description. CFD-DEM simulations can provide a deeper insight in the particle fluid dynamics in the outlet regions (Kerst et al., 2016); they may help to validate and to improve the process model presented here. Second, the current model does not allow predicting the purity of the product. Therefore, nucleation of the counter-enantiomer and solubility properties of ternary systems will be included in a future version of the model.

The simulations in this paper throw only spotlights on a few points in a high-dimensional parameter space. An optimal choice of operation and design parameters will require a systematic mathematical optimization. This will be done in our future work using the model reduction approaches presented in (Mangold et al., 2015; Feng et al., 2016).

**Acknowledgements**

This work has been supported financially by DFG in the framework of SPP 1679.

## Appendix A. Identification of kinetic parameters of the mill model

During the mill identification experiments, the liquid flow rate $\dot{V}_{in}$ through the crystallizer is set to zero, i.e. particles coming out of the disperser are directly

recycled into the disperser. The particle size distribution at the disperser outlet was measured optically at discrete time points $t_i$ with an interval of about 30 s.

In the context of the crystallization process, the mill model is to capture two main effects of the disperser on the system: The mass ratio between small particles (with $L < L_c$) and large particles (with $L > L_c$) at the outlet of the disperser

$$y_1(t_i) = \frac{\int_0^{L_c} n_M(L, t_i)\ L^3\ dL}{\int_{L_c}^{\infty} n_M(L, t_i)\ L^3\ dL}, \tag{A.1}$$

and the average size of the generated small particles

$$y_2(t_i) = \frac{\int_0^{L_c} n_M(L, t_i)\ L\ dL}{\int_{L_c}^{\infty} n_M(L, t_i)\ dL}. \tag{A.2}$$

The unknown kinetic parameters $p$, $q$, $S_0$ are obtained from a maximum likelihood estimation by minimizing

$$\chi^2(p, q, S_0) = \sum_i w\ \left(\frac{y_1(t_i) - \hat{y}_1(t_i; p, q, S_0)}{\sigma_1}\right)^2 + (1-w)\ \left(\frac{y_2(t_1) - \hat{y}_2(t_1; p, q, S_0)}{\sigma_1}\right)^2, \tag{A.3}$$

where the $\hat{}$ -sign denotes a simulated value.

Application of the profile likelihood method (Murphy and van der Vaart, 2000; Raue et al., 2009) confirms practical identifiability of the three kinetic parameters.

Figure A.16 shows that a reasonable agreement between model and experimental data is reached. The identified parameter values are listed in Table 1.

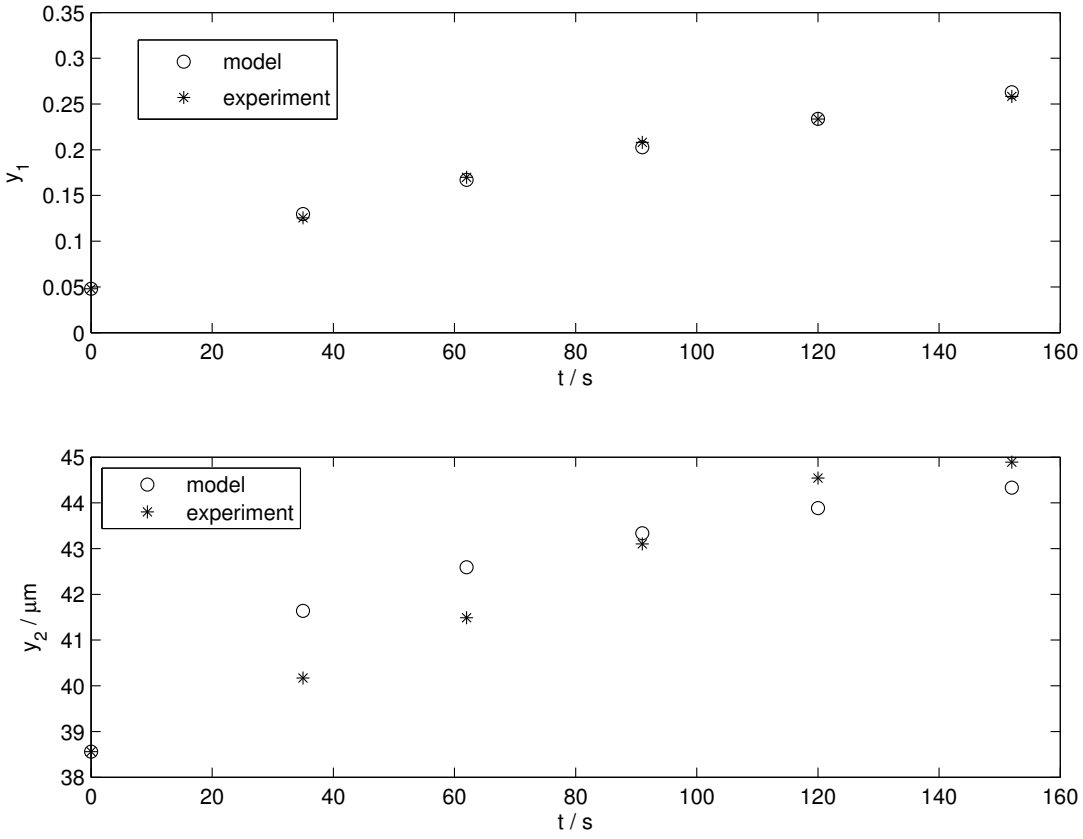


Figure A.16: Comparison between disperser model and experimental data after fitting the kinetic parameters $p$, $q$, $S_0$

## References


Alvarez, A., Myerson, A., 2010. Continuous plug flow crystallization of pharmaceutical compounds. Crystal Growth & Design 10, 2219–2228.

Binev, D., 2015. Continuous fluidized bed crystallization. Ph.D. thesis, Otto von Guericke University, Magdeburg.

Binev, D., Seidel-Morgenstern, A., Lorenz, H., 2015. Study of crystal size distributions in a fluidized bed crystallizer. Chemical Engineering Science 133, 116–124.

Binev, D., Seidel-Morgenstern, A., Lorenz, H., 2016. Continuous separation of isomers in fluidized bed crystallizers. Crystal Growth & Design 16, 1409–1419.

Diemer, R., Spahr, D., Olson, J., Magan, R., 2005. Interpretation of size reduction data via moment models. Powder Technology 156, 83–94.

Feng, L., Mangold, M., Benner, P., 2016. Adaptive POD-DEIM basis construction and its application to a nonlinear population balance system. AIChE Journal (submitted).

Galan, K., Eicke, M., Elsner, M., Lorenz, H., Seidel-Morgenstern, A., 2015. Continuous preferential crystallization of chiral molecules in single and coupled mixed-suspension mixed-product-removal crystallizers. Crystal Growth & Design 15, 1808–1818.

Gibilaro, L., 2001. Fluidization-dynamics: the formulation and applications of a predictive theory for the fluidized state. Butterworth-Heinemann.

Hill, P., Ng, K., 1996. Statistics of multiple particle breakage. AIChE Journal 42, 1600–1611.

Kerst, K., Roloff, C., de Souza, L. M., Bartz, A., Seidel-Morgenstern, A., Thévenin, D., Janiga, G., 2016. CFD-DEM simulations of a fluidized bed crystallizer. Chemical Engineering Science (submitted).

Lorenz, H., Seidel-Morgenstern, A., 2014. Processes to separate enantiomers. Angewandte Chemie International Edition 53 (5), 1218–1250.

Luciani, C., Conder, E., Seibert K., 2015. Modeling-aided scale-up of high-shear rotorstator wet milling for pharmaceutical applications. Organic Process Research & Development, 582–589.

Mangold, M., Feng, L., Khlopov, D., Palis, S., Benner, P., Binev, D., Seidel-Morgenstern, A., 2015. Nonlinear model reduction of a continuous fluidized bed crystallizer. Journal of Computational and Applied Mathematics 289, 253–266.

Midler, M., 1975. Process for production of crystals in fluidized bed crystallizers. United States Patent no. 3892539.

Midler, M., 1976. Crystallization system and method using crystal fracturing external to a crystallization column. United States Patent no. 3996018.

Murphy, S., van der Vaart, A., 2000. On profile likelihood. Journal of the American Statistical Association 95, 449–477.

Myerson, A., 2002. Handbook of Industrial Crystallization, 2nd Edition. Butterworth-Heinemann, Boston.

Palis, S., Binev, D., Lorenz, H., Seidel-Morgenstern, A., Kienle, A., 2013. Population balance modeling of crystallization in a fluidized bed. In: BIWIC 2013 20th International Workshop on Industrial Crystallization. pp. 252–259.

Qamar, S., Galan, K., Elsner, M., Hussain, I., Seidel-Morgenstern, A., 2013. Theoretical investigation of simultaneous continuous preferential crystallization in a coupled mode. Chemical Engineering Science 98, 25-39.

Raue, A., Kreutz, C., Maiwald, T., Bachmann, J., Schilling, M., Klingmüller, U., Timmer, J., 2009. Structural and practical identifiability analysis of partially observed dynamical models by exploiting the profile likelihood. Bioinformatics 25, 1923–1929.

Reynolds, G., 2010. Modelling of pharmaceutical granule size reduction in a conical screen mill. Chemical Engineering Journal 164, 383–392.

Richardson, J., Zaki, W., 1954. Sedimentation and fluidization: Part I. Chemical Engineering Science 3, 65–73.

Stinson, S., 2001. Chiral pharmaceuticals. Chemical Engineering News 79 (40), 79–97.

Vetter, T., Burcham, C., Doherty, M., 2015. Separation of conglomerate forming enantiomers using a novel continuous preferential crystallization process. AIChE Journal 61 (9), 2810–2823.

## List of Symbols

*Latin symbols:*

| *symbol* | *description* | *unit* |
|---|---|---|
| $A$ | cross-sectional area | $\mathrm{m}^2$ |
| $D$ | dispersion coefficient | $\mathrm{m}^2\,\mathrm{s}^{-1}$ |
| $d$ | diameter | m |
| $d_B$ | diameter at the bottom of the crystallizer | m |
| $d_T$ | diameter at the top of the crystallizer | m |
| $G$ | particle growth rate | $\mathrm{m}\,\mathrm{s}^{-1}$ |
| $G_0$ | particle growth rate constant | $\mathrm{m}\,\mathrm{s}^{-1}$ |
| $\mathrm{m}\,\mathrm{s}^{-1}$ | | |
| $H$ | height of crystallizer | m |
| $L$ | internal coordinate / particle diameter | m |
| $L_C$ | critical breakage size | m |
| $n(x, L, t)$ | number size density crystallizer | $\mathrm{m}^{-3}_{suspension}\,\mathrm{m}^{-1}$ |
| $n_M(L, t)$ | number size density mill | $\mathrm{m}^{-3}_{suspension}\,\mathrm{m}^{-1}$ |
| $p$ | kinetic parameter in breakage distribution function | |
| $q$ | kinetic parameter in breakage distribution function | |
| $S_0$ | kinetic parameter in breakage kernel | |
| $t$ | time | s |
| $V_M$ | volume of particle mill | $\mathrm{m}^3$ |
| $\dot{V}_{in}$ | volume flow into the crystallizer | $\mathrm{m}^3\,\mathrm{s}^{-1}$ |
| $\dot{V}_M$ | volume flow to / from the particle mill | $\mathrm{m}^3\,\mathrm{s}^{-1}$ |
| $\dot{V}_{prod}$ | product volume flow | $\mathrm{m}^3\,\mathrm{s}^{-1}$ |
| $v_P$ | particle velocity | $\mathrm{m}\,\mathrm{s}^{-1}$ |
| $x$ | space coordinate | m |
| $x_c$ | position between cylindrical part and conical part of the crystallizer | m |
| $x_M$ | position of the connection between crystallizer and mill | m |
| $x_P$ | position of the product outlet | m |

*Greek symbols:*

| *symbol* | *description* | *unit* |
|---|---|---|
| $\epsilon$ | volume fraction of the fluid | |
| $\mu_f$ | dynamic viscosity | $\mathrm{kg\,m^{-1}\,s^{-1}}$ |
| $\rho_F$ | fluid density | $\mathrm{kg\,m^{-3}}$ |
| $\rho_P$ | particle density | $\mathrm{kg\,m^{-3}}$ |
| $\sigma$ | supersaturation | |
| $\Psi$ | sphericity parameter | |